SCIENCE CHINA
Physics, Mechanics & Astronomy

• Article •

January 2012 Vol.55 No.1: 118–124
doi: 10.1007/s11433-011-4535-2

Dynamic mode decomposition of hairpin vortices generated by a hemisphere protuberance

TANG ZhanQi[1] & JIANG Nan[1,2*]

[1] *Department of Mechanics, Tianjin University, Tianjin 300072, China;*
[2] *Tianjin Key Laboratory of Modern Engineering Mechanics, Tianjin 300072, China*

Received July 8, 2011; accepted September 23, 2011; published online October 26, 2011

We present dynamic mode decomposition (DMD) for studying the hairpin vortices generated by hemisphere protuberance measured by two-dimensional (2D) time-resolved (TR) particle image velocimetry (PIV) in a water channel. The hairpins dynamic information is extracted by identifying their dominant frequencies and associated spatial structures. For this quasi-periodic data system, the resulting main Dynamic modes illustrate the different spatial structures associated with the wake vortex region and the near-wall region. By comparisons with proper orthogonal decomposition (POD), it can be concluded that the dynamic mode concentrates on a certain frequency component more effectively than the mode determined by POD. During the analysis, DMD has proven itself a robust and reliable algorithm to extract spatial-temporal coherent structures.

hairpin vortices, hemisphere protuberance, time-resolved particle image velocimetry, dynamic mode decomposition, proper orthogonal decomposition

PACS number(s): 47.15.Cb, 47.27.De, 47.32.C2, 47.80.Cb

Citation: Tang Z Q, Jiang N. Dynamic mode decomposition of hairpin vortices generated by a hemisphere protuberance. Sci China-Phys Mech Astron, 2012, 55: 118–124, doi: 10.1007/s11433-011-4535-2

Hairpin vortexes as the common elementary characteristic exist in the turbulent boundary layer. The primary hairpin can generate more offspring hairpins according to the parent-offspring scenario to form the hairpin vortex packets, which always appear in the low speed region between the hairpin legs. Smith and Walker [1] explained that the bursting process of streaks feeds concentrated vorticity into the outer layer, thus providing a feedback mechanism to strengthen the regeneration process of hairpin packets. In this way, hairpin packets prevail in the outer part of the boundary layer, and meanwhile, long and large-scale streaky structures occupy the inner part, which would make up the skeleton frame and foundation of a self-sustained turbulent boundary layer. Clearly, the hairpin vortices are so important in the boundary layer that the study of discrete hairpin vortices and their induced flow patterns in an initially stable boundary layer is necessary. Figure 1 shows a sketch of the hairpins generated by the hemisphere protuberance [2].

The search for physical mechanisms underlying fluid

Figure 1 A sketch of the hairpins generated by the hemisphere protuberance [2].

---

*Corresponding author (email: nanj@tju.edu.cn) flow relies on the decomposition of flow fields into coherent structures and flow patterns whose dynamics provides a more compact and instructive manner of describing the fluid process. Dynamic mode decomposition (DMD) was recently developed based on Koopman analysis [3] of dynamical system by Schmid et al. [4]. This technique uses snapshots of the flow field only, and is capable of describing the flow elements that characterize the dominant dynamic behavior without any recurrence to the underlying governing equations [4]. DMD provides a more compact and instructive manner of understanding the fluid process by revealing dynamic information of the flow field, e.g. the temporal dynamics and the associated spatial shapes in a temporally orthogonal sense.

In the present paper, a two-dimensional (2D) time-resolved (TR) PIV study is done to investigate the hairpin vortices generated by the interaction of a hemisphere protuberance within a developing laminar boundary layer from the side view and the top view, respectively. After acquiring the basic spatial-temporal velocity information, then DMD is used to extract the hairpins' dynamic information by identifying the dominant frequencies and the associated spatial structures. Additionally, the comparison between the methods of DMD and POD will also be presented.

1 Experimental set-up and method

1.1 Experimental set-up

The present experiment is carried out in a re-circulating water channel. The water-channel system has a working section 1200 mm long, 150 mm wide, and 140 mm deep, with an operating velocity of 10 cm/s for the present experiment. A 1000 mm long Plexiglas flat with a 4:1 elliptical leading edge is utilized as a test surface. The plate is supported 15 mm above the channel surface by adjustable legs to allow the development of a laminar boundary layer and to prevent interference by channel-wall boundary layers. Hairpin vortices are generated by three-dimensional vortex shedding from hemisphere protuberance with the height h = 9 mm placed at a distance of 150 mm downstream along the leading edge of the plate. The boundary layer thickness just upstream of the hemisphere is about δ/h=1, Re_h=800.

A 2D TR PIV system is based on practical Nd:Yag lasers and a high speed camera is utilized for particle images recording, storage and processing. A schematic diagram of the test system is shown in Figure 2. Seeding particles with a median diameter of 10 μm and density of 1.03 g/mm^3 are illuminated by a laser sheet with a thickness of about 1 mm. 2D TR PIV measurement is taken in the streamwise-normal wise (x, y)-plane and the streamwise-spanwise (x, z)-plane, separately. For the side-view case, the laser plane crosses the axial center-plane of the hemisphere along the streamwise direction. A high-speed camera (1280 pixels × 1024 pixels) acquires the particle images in the (x, y)-plane from a side view; then, the velocity data in the (x, z)-plane parallel to the wall of the plate at a height (y/h= 5/6) are obtained for the top view case (shown in Figure 2(b)).

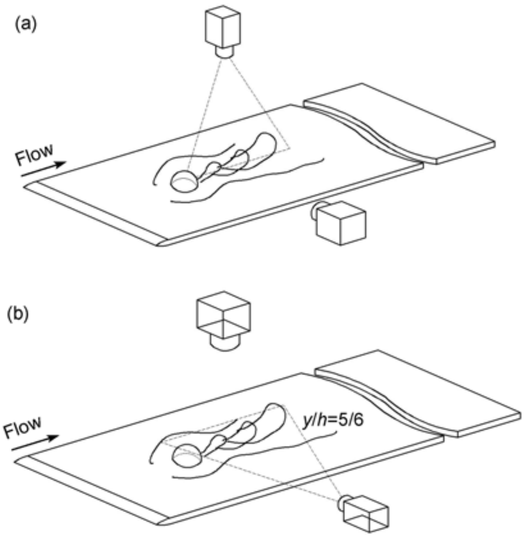

Figure 2 Schematic diagram of the hairpins generation and experimental set-up. (a) Side view; (b) top view.

The present sampling frequency of the camera is 250 Hz. 6548 snapshots of particle images are recorded for each region, and are analyzed by the following steps: background subtraction, adaptive correlation with inter-rogation windows of 32 pixels×32 pixels and an overlap rate of 75%, range validation and the last step of average filter. Each flow field consists of 157×125 two-dimensional velocity vectors. The field is about 120 mm×95 mm (streamwise length× wall-normal height/spanwise width).

1.2 Principles of the dynamic mode decomposition

After acquiring the velocity data, the dynamic mode decomposition (DMD) method is used for data processing. The basic concept, fundamental mathematical deduction, and physical explanation of DMD have been given by Schmid et al. [4] and Pan et al. [5]. Here, we just give a brief explanation of the DMD method for our present experiment. The DMD does not depend on a particular basis model; however, its reliance on data allows a time-resolved sequence of flow field measurements that suffice to perform the dynamic mode decomposition. In the present experiment, we assume general flow field data and denote each such field by a vector v_j. A sequence of N snapshots is then written as $V_1^N = \{v_1, v_2, \cdots, v_N\}$, where an equal time interval Δt is assumed between two subsequent snapshots v_j and v_{j+1}. These snapshots v_j should be produced by a nonlinear process for experimental data. However, for the purpose of invoking a linear-tangent approximation, a linear mapping $\boldsymbol{A}$ from one snapshot to the next is employed. This mapping is taken as a constant over all the data sequence which is written as $\boldsymbol{v}_{j+1}=\boldsymbol{A}\boldsymbol{v}_j$. Following the idea underlying the Arnoldi method (Greenbaum [6]; Trefethen and Bau [7]), the linear map $\boldsymbol{A}$ could be expressed as $V_2^N=\boldsymbol{A}V_1^{N-1}\approx V_1^{N-1}\boldsymbol{S}$, with $\boldsymbol{S}$ as a companion matrix that simply shifts the snapshots 1 through N–1 (via the subdiagonal matrix entries) and approximates the last snapshot N by a linear combination of the previous N–1 snapshots [8]. As the number of snapshots increases and the data sequence given by V_1^{N-1} captures the dominant features of the underlying physical process, it is reasonable to assume that, beyond a critical number of snapshots, the vectors could become linearly dependent. This procedure will result in the low-dimensional system matrix $\boldsymbol{S}$. The matrix $\boldsymbol{S}$ can be computed from the above equation by a least-squares approximation based on the two data sets V_1^{N-1} and V_2^N, as $S=R^{-1}Q^HV_2^N$, with $V_1^{N-1}=QR$ as the QR-decomposition of V_1^{N-1}. It is noted that at no point in the above procedure do we need the explicit form of the system matrix $\boldsymbol{A}$. Only its low-dimensional proxy $\boldsymbol{S}$ is required. It is then known that the eigenvalues of $\boldsymbol{S}$ approximate some of the eigenvalues of $\boldsymbol{A}$ and the corresponding eigenvectors of $\boldsymbol{A}$ are determined by $DM_j=V_1^{N-1}w_j$, where w_j is an eigenvector of $\boldsymbol{S}$ to the nature of the data sequence. The eigenvalues λ of $\boldsymbol{S}$ describe the inter-snapshot dynamics, in accordance with the standard convention. The eigenvalues of $\boldsymbol{S}$ are logarithmically mapped onto the complex plane: $\omega=\log(\lambda)/\Delta t=\omega_r+\omega_i$, in which their real part ω_r represents exponential growth or decay (depending on the sign) and their imaginary part ω_i contains the temporal frequency. The associated eigenvectors of $\boldsymbol{S}$ provide the coefficients of the linear combination that is necessary to express the modal structure within the snapshot basis. In order to evaluate the dominance between dynamic modes, we can project a specific dynamic mode DM_j onto the proper orthogonal decomposition (POD) basis, form the modulus of the resulting vector [4], and use it as a criterion to rank dynamic modes, similar to ranking POD modes with energy content.

After describing the experimental setup and the principles of the dynamic mode decomposition, a set of 2D TR PIV-measurements will be processed and analyzed. The obtained results will be presented in the form of their spectral characteristics (frequencies and amplitudes) and modal shapes. Additionally, the comparison with the POD method will be also illustrated in this paper.

2 Results and analysis

The instantaneous flow field in the wake region of the hemisphere protuberance from the side view is shown in Figure 3. The vector field which subtracts the local convectional velocity (mean velocity) is shown, clearly four clockwise swirling motions marked by red circles appear in the wake shear layer downstream along the hemisphere protuberance. In the plot, the closed streamlines representing the heads of the vortexes and Q2 event just upstream and below the head are consistent with the key features of the hairpin vortex. Moreover, as the model of the hairpins is generated by the hemisphere protuberance (shown in Figure 1) given by Acarlar and Smith [2], this succession of swirling motions (red circles) correspond to the heads of the succession of hairpins shedding from the hemisphere. As shown in the plot, these hairpins are growing upward convecting along the streamwise direction, and then several hairpin heads appear with an inclination angle with the wall.

2.1 DMD modes and frequencies

For the present experiment, the DMD temporal analysis is attempted with a sequence of flow fields:

$$\{v_1,v_2,\dots,v_N\}=\{v\ (t=2\Delta t),v\ (t=4\Delta t),\cdots v\ (t=6000\Delta t)\}$$

with N=3000 in time. These 3000 time-step flow fields could be reshaped into the columns of a data matrix V_1^{3000}, and the corresponding companion $\boldsymbol{S}$-matrix of dimension 2999×2999 can be deduced following the procedure described above, whose eigenvalues are shown in Figure 4(a). Figure 4(a) shows that nearly all the eigenvalues are expected to tend towards on the unit circle $\left|\lambda_j\right|=1$ suggesting that most modes are quasi-neutral stable, while those dynamic modes fallen inside the unit circle might have resulted from contamination of measurement noise. In all these dynamic modes, the mean flow mode (1.000018, 0) signifying the temporally-averaged flow field of the data sequence has been omitted in the Figure, and the other four main eigenvalues are distinguished in color blue, depending on the magnitude of the corresponding Dynamic mode. The magnitudes defined by the global energy norm $\left\|v_j\right\|$ are shown in Figure 4(b) with the same color as the spectrum. In Figure 4(b) each mode is displayed with its magnitude at its corresponding frequency (f) expressed as the image part of ω_j normalized by 2π in the current case. As the eigenvalues appear in complex conjugate pairs, only the cases of f>0 (ω_j>0) are shown and the mean flow mode at f = 0 is not displayed. By ordering the modes with respect to their magnitude plotted in the Figure 4(b), two pronounced peaks at two frequencies can be observed: the first and second modes oscillate with f_1=1.766 and f_2=2.606 respectively. However two modes (3rd and 4th) with a relative low frequency (f_3= 0.8400; f_4= 0.7413) are also extracted. It can be seen that the linear combinations of the first and third modes excite the second (higher) mode ($f_2=f_1+f_3$).

Acarlar and Smith [2] experimentally explain that the periodicity of the vortex shedding from hemispheres was examined over a wide Reynolds number range. In the current

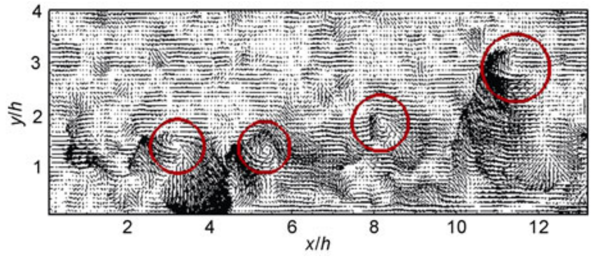

Figure 3 Snapshot of the instantaneous fluctuation vector for the side-view case.

experiment, the two distinct time series at two different positions in the region are chosen for further discussion: one is in the shedding vortex region along the wake trajectory ($\boldsymbol{x}_1$(x/h, y/h)=(4, 1.7)), and the other one is located just downstream of the hemisphere and close to the wall ($\boldsymbol{x}_2$(x/h, y/h)=(4, 0.3)). Figure 5(a) shows the power spectrum of time signal at $\boldsymbol{x}_1$ (black line). The peak frequency corresponds to a vortex shedding of wake vortices with $f_{x_1}=1.766$ Hz. In Figure 5(b), the peak frequency of the time signal located at $\boldsymbol{x}_2$ oscillates with $f_{x_2}=0.80189$ Hz, much smaller than the shedding frequency f_{x_1}. In the whole region we measured, it is noted that the peak frequencies of the power spectra vary with the different locations in the region downstream of the hemisphere protuberance, the whole motion in the region we covered is integrated by multi-frequencies cases working together.

As stated above, the image part of ω_j normalized by 2π could reveal the frequency of the corresponding dynamic mode. In Figures 5(a) and 5(b) the power spectra of the two time signals (black lines) are compared with the frequencies obtained directly from the eigenvalues of the $\boldsymbol{S}$-matrix (blue vertical lines, also shown in Figure 4(b)). The shedding frequency and the lower harmonic are in agreement with the frequencies of the main dynamic modes, although the sample frequency of the two extracted time series is just 250 Hz. As shown, the dominant dynamic eigenvalues match the frequencies for the shear-layer mode ($f_{x_1}=1.766$) and the wall mode ($f_{x_2}=0.80189$). It should be noted that in the current experiments the time signals are local measures of the frequencies at one spatial point. However, the frequency of time signal at two different local spatial locations is separately extracted. The dynamic eigenvalues correspond to the global region in the flow fields with time-periodic motion. Moreover, we can also obtain that DMD is capable of distinguishing the different dynamic modes by the spectra of frequency.

Figure 6 shows the dynamic modes corresponding, respectively, to the three main frequencies indicated in color blue in the amplitude plot (Figures 4(b) and 5). All modes are visualized by the streamwise velocity contour in the

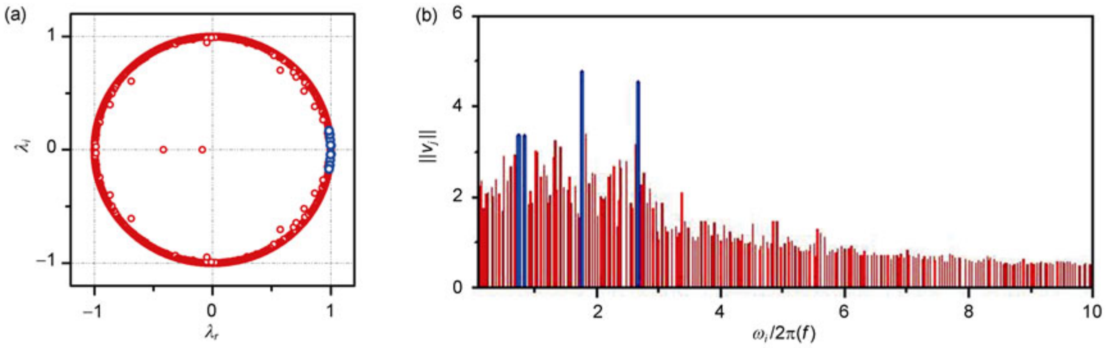

Figure 4 (a) Eigenvalues λ_j of the matrix $\boldsymbol{S}$ representing the inter-snapshot dynamics. The values corresponding to the four main dynamic modes are shown with the blue symbol; (b) the magnitudes of the dynamic modes at each frequency.

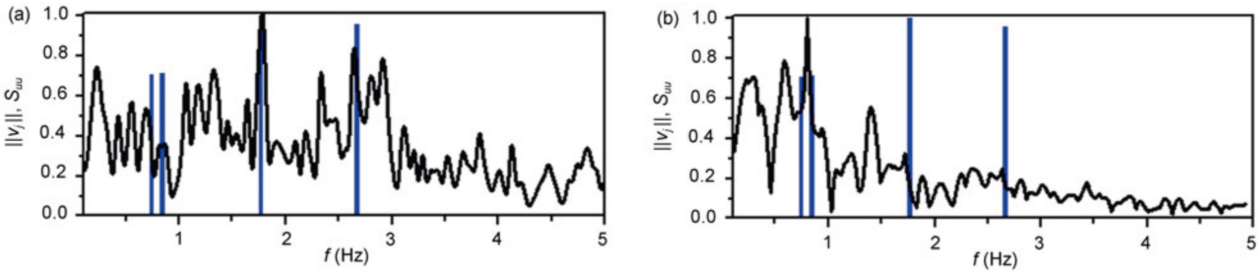

Figure 5 The spectral contents of two time signals located (a) in the wake vortex region $\boldsymbol{x}_1$(x/h, y/h)=(4, 1.7) and (b) near the wall $\boldsymbol{x}_2$(x/h, y/h)=(4, 0.3) are shown in color black and the magnitudes of the first four of DMD modes at each frequency are shown in blue. The amplitudes are normalized with their maximum values.

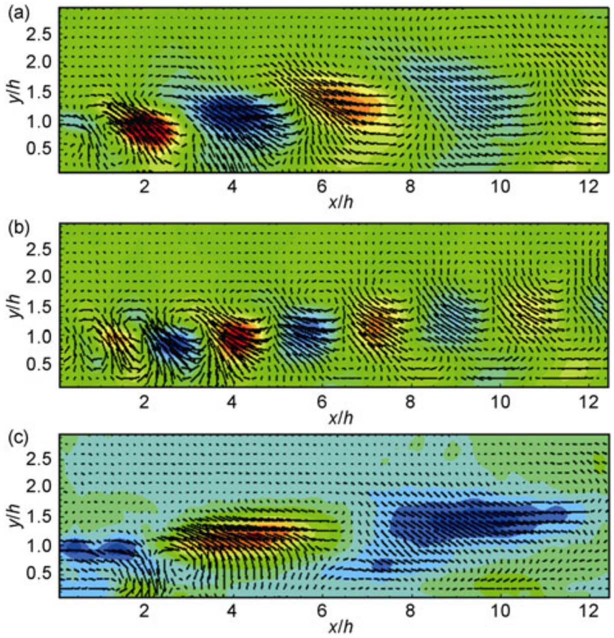

Figure 6 The contour levels of the streamwise velocity components of three main dynamic modes. (a) First mode, with $\|DM_2\|$=4.76873 and f_1=1.766; (b) second mode, with $\|DM_2\|$=4.55883 and f_2=2.606; (c) third mode, with $\|DM_3\|$=3.38412 and f_3=0.8400.

(x, y)-plane. In these modes (with frequency f_1 =1.766 Hz, f_2 =2.606 Hz, f_3 =0.8400 Hz), the three successions of vortexes inclined with the wall along the streamwise direction can be extracted, due to the rise of hairpins heads generated by the hemisphere protuberance as they are evolving downstream. This is similar to the instantaneous results shown in Figure 3. Also, the density of the vortex structures for different modes demonstrates that the temporal dynamic mode decomposition can indeed identify distinct frequencies underlying the data sequence. The first mode f_1 (Figure 6(a)) can be associated with the primary vortex shedding frequency, which is consistent with the experimental work by Acarlar and Smith [2]; the low frequency mode f_3 shown in Figure 6(c) features large-scale positive and negative streamwise velocities, which can be associated with another kind of wall vortex structure in the near wall region induced by the primary hairpin vortexes of the first mode f_1. In addition, the linear combinations of the frequencies can excite the higher modes f_2, as shown in Figure 6(b). The nonlinear interaction of f_1 and f_3 results in f_2, representing the higher-order harmonics in the measured region.

We also analyze the streamwise-spanwise plane flow field by DMD as stated above. Figure 7 shows the velocity vectors of the first mode (except the mean flow mode), with the frequency f_1 =1.76 Hz indicating the shedding frequency of hairpin legs, which is consistent with the frequency of the first mode for the side-view case. In the plot, the counter-rotating vortex pairs with an increasing spanwise width organized in the streamwise direction, which correspond with the cross-section of a succession of hairpin legs in the streamwise-spanwise (x, z)-plane. Combining the side-view and top-view results, we can reconstruct the spatial shape of the series of hairpins generated by the hemisphere: the hairpin heads are rising up and legs are being apart along the streamwise direction, evolving into a larger hairpin body downstream.

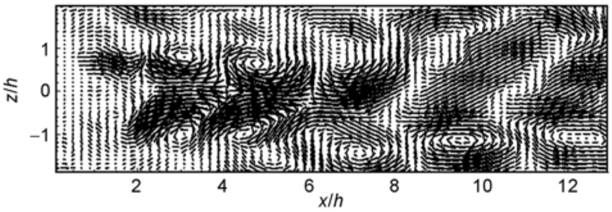

Figure 7 Decomposition of the flow field in the (x, z)-plane from the top-view with the most dominant dynamic mode (except mean flow mode).

2.2 Comparison with POD modes

So far, many other techniques have been developed to extract coherent motion in a more general way, in which the POD technique, first introduced by Lumley [9] in the context of coherent structures, has been also increasingly applied in conjunction with PIV. Used with POD, the measurements yield optimal basis functions for a given flow field (e.g., Lumley [9]; Sirovich [10]; Berkooz et al. [11]; Holmes et al. [12]).

For the above side-view experimental data and for comparison purposes in the following, the POD analysis uses the set of flow fields at discrete times:

$$\left\{v\ (t=2\Delta t), v\ (t=4\Delta t), \cdots, v\ (t=6000\Delta t)\right\},$$

which have been performed in DMD analysis. The results of POD analysis are displayed in Figure 8. The energy spectrum shown in Figure 8(a), shows a rather weak decay after the first initial drop. The first POD mode, corresponding to the largest singular value, represents the mean flow, the same as the mean flow DMD mode. The result of most energetic POD mode (except mean flow mode) shown in Figure 8(b) captures similar spatial structures to the most main dynamic mode shown in Figure 6(a). However, the downstream region is significantly different from the DMD mode, which will be discussed later.

For further comparison, we need consider the temporal behavior of the main POD and DMD modes (both except the mean flow mode). The temporal behavior of the main POD mode is characterized by computing the POD coefficients via projecting the flow-field snapshots onto the corresponding mode. Mezić & Banaszuk [13] and Mezić [14] discussed that in spite of the periodic or non-periodic systems, the flow field can be reconstructed with isolated DMD modes by discrete Fourier transformation:

$$v_k = \sum_{j=0}^{N-1} \mathrm{e}^{2\pi ijk/N} v_j,\ k = 0, \cdots, N-1,$$

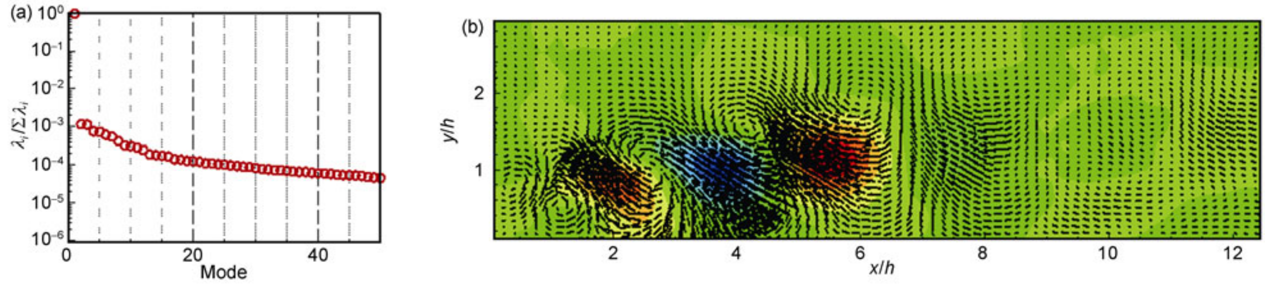

Figure 8 (a) Energy spectra from the (x, y)-plane velocity POD decomposition; (b) the stream-wise component of the most energetic POD mode (except the mean flow mode).

and the DMD coefficient takes the form as $a(t)=\mathrm{e}^{\omega t}$, where $\omega\approx 1.766i$ for the main dynamic mode. The distinction in the time coefficients between POD and DMD is shown in Figure 9(a), where the main Dynamic mode contains only a single frequency component, and presents periodical variation with an amplitude fixed over periods. In contrast, the concerning POD mode results in the mode that looks like containing several frequencies. All of these become clear in the spectrum of the coefficients as shown in Figure 9(b): the power spectrum of DMD coefficients with a distinct peak is expected at f=1.76. However, the coefficient of the POD mode oscillates with multi-frequencies, although undulating with a frequency f=1.79167 close to the frequency extracted by the main DMD mode. The two higher frequencies are also extracted, which cause the beating shown in Figure 9(a), and the velocity of this POD mode could be contaminated when these frequencies work together, just as the streamwise velocity component in the downstream region plotted in the Figure 8(b).

The dynamic mode decomposition is capable of extracting dominant flow features from the velocity field basis, by approximating the linear mapping between the velocity fields. In contrast, POD uses a second-order statistics of the flow fields and produces a hierarchy of coherent structures that diagonalize their correlation tensor. It can be said that POD concentrates on a representation based on the spatial orthogonality, and DMD focuses on a representation based on the temporal orthogonality (frequencies), when the spatial relationship is taken into account between the various parts of the whole region we covered. By comparison, we conclude that the DMD modes are thus more effective at decoupling and isolating these dynamics.

3 Conclusions

In this paper, we have presented Dynamic Mode Decomposition for studying the periodic dynamical behavior of the hairpin vortexes generated by hemisphere protuberance. The nonlinear dynamical system is acquired by 2D TR PIV from the side view and the top view, separately. DMD is used to extract the dynamic information by identifying the dominant frequencies and their associated spatial structures. The resulting main modes illustrate the different spatial structures associated with the wake vortex region and the near-wall region, which indicates that DMD provides a

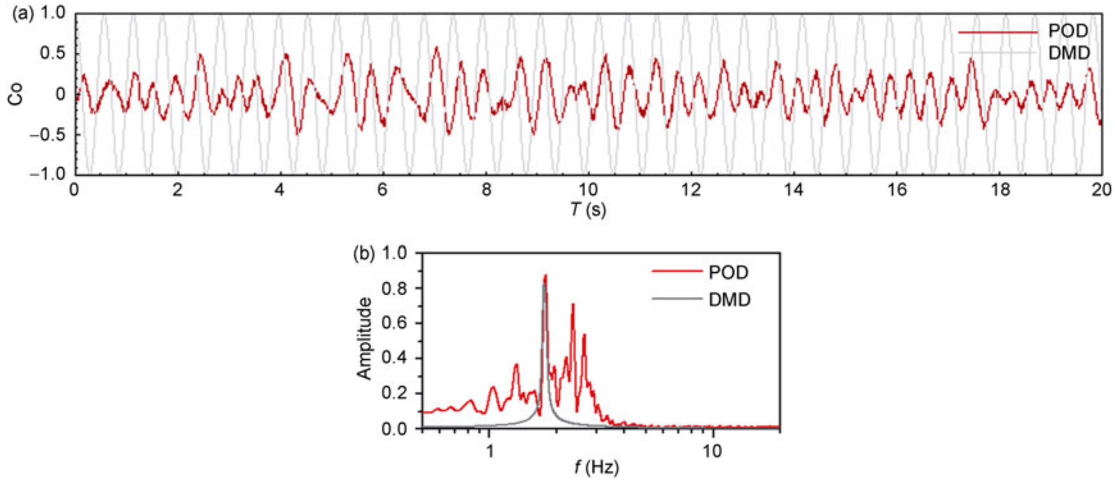

Figure 9 (a) Comparison of the temporal behavior of time coefficients: the most energetic POD mode (red), and the coefficient of the main dynamic mode (grey); (b) the power spectrum of the corresponding time coefficient is shown with the same color.

method to extract the main frequencies in the different parts of the whole region we covered, and also offer the linear combined result of these separated main modes.

Additionally, by comparing the coefficients of the main DMD and POD modes (except the mean flow mode), the most striking distinction is shown in the time coefficients. A single DMD mode contains only a single centralized frequency component, while the POD mode captures the most energetic structures as a combination of several significant frequency components (shown in Figure 9(b)). The experimental evidence also shows that hairpin vortexes shed from the hemisphere protuberance at a definite frequency instead of several frequencies, which is in agreement with the single frequency property of DMD in temporal behavior. However, the POD modes could not exhibit this ability. Thus, it can be concluded that dynamic modes are more effective at isolating these dynamics concentrating on a certain frequency component in temporal behavior than the modes determined by POD.

In short, for the above case of the flow generated by hemisphere protuberance, DMD produces an effective description of the flow behavior, capable of identifying dynamic features directly.

This work was supported by the National Natural Science Foundation of China (Grant Nos. 10832001 and 10872145) and the State Key Laboratory of Nonlinear Mechanics, Institute of Mechanics, Chinese Academy of Sciences.

1 Smith C R, Walker J D A. Sustaining mechanisms of turbulent boundary layers: The role of vortex development and interactions. In: Self-Sustaining Mechanisms of Wall Turbulence. Boston: Computational Mechanics, 1997. 13–47

2 Acarlar M S, Smith C R. A study of hairpin vortices in a laminar boundary layer. Part 1: Hairpin vortices generated by a hemisphere protuberance. J Fluid Mech, 1987, 175: 1–41

3 Rowley C, Mezic I, Bagheri S, et al. Spectral analysis of nonlinear flows. J Fluid Mech, 2009, 641: 115–127

4 Schmid P J. Dynamic mode decomposition of numerical and experimental data. J Fluid Mech, 2010, 656: 5–28

5 Pan C, Yu D S, Wang J J. Dynamical mode decomposition of Gurney flap wake flow. Theor Appl Mech Lett, 2011, 1: 012002

6 Greenbaum A. Iterative Methods for Solving Linear Systems. Philadelphia: SIAM, 1997

7 Trefethen L N, Bau D. Numerical Linear Algebra. Philadelphia: SIAM, 1997

8 Ruhe A. Rational Krylov sequence methods for eigenvalue computation. Lin Alg Appl, 1984, 58: 279–316

9 Lumley J L. The structure of inhomogeneous turbulent flows. In: Proceedings of the International Colloquium on the Fine Scale Structure of the Atmosphere and its Influence on Radio Wave Propagation. Moscow: Nauka, 1967. 166–178

10 Sirovich L. Turbulence and the dynamics of coherent structures. Q Appl Math, 1987, 45: 561–590

11 Berkooz G, Holmes P, Lumley J L. The proper orthogonal decomposition in the analysis of turbulent flows. Annu Rev of Fluid Mech, 1993, 25: 539–75

12 Holmes P, Lumley J L, Berkooz G. Turbulence, Coherent Structures, Dynamical Systems and Symmetry. Cambridge: Cambridge University Press, 1996

13 Mezić I, Banaszuk A. Comparison of systems with complex behaviour. Physica D, 2004, 197: 101–133

14 Mezić I. Spectral properties of dynamical systems, model reduction and decompositions. Nonlinear Dyn, 2005, 41: 309–325